IEEE Access
Multidisciplinary | Rapid Review | Open Access Journal

Date of publication xxxx 00, 0000, date of current version xxxx 00, 0000.

Digital Object Identifier 10.1109/ACCESS.2017.Doi Number

Research on Active Obstacle Avoidance Control Strategy for intelligent vehicle based on active safety collaborative control

Haiqing Li[1], Member, IEEE, Jing Li[1], Zuqiang Su[1], Xin Wang[1], and Jiufei Luo[1]
[1] School of Advanced Manufacturing Engineering, Chongqing University of Posts and Telecommunications, Chongqing 400065, China;

Corresponding author: Haiqing Li (lihq@cqupt.edu.cn).

This work was supported in part by the National Natural Science Foundation of China under Grant 51705059 and 51705060, the Basic Research and Frontier Technology of the Chongqing Science and Technology Commission under Grant cstc2020jcyj-msxm1768, and the Fundamental Research Funds for the Central Universities under Grant E012A2020024.

ABSTRACT Aiming at the issue of active obstacle avoidance control for intelligent vehicles under emergency, an active safety collaborative control system integrated with adaptive cruise control (ACC), rear steering control (RSC), and rollover braking control (RBC) is developed. The proposed novel control architecture consists of a supervisor, an upper controller, and a lower controller. The supervisor decides which control mode to be used based on multi-sensors information of the driving vehicle. Active rear wheel steering based on lateral acceleration feedback and active braking control strategies based on fuzzy PID are added into the control model to enhance driving stability. To make the vehicle motion control model suitable for highway path tracking with obstacle avoidance under emergency, a priority is given to the RBC controller even though the vehicle speed is lower than the expected speed when the rollover index exceeds the safety threshold. A nonlinear vehicle simulation model is established to validate the proposed control scheme based on Carsim. Finally, a Carsim-Simulink co-simulation model is constructed, and simulation results show that the proposed integrated control strategy based on active safety collaborative control has good performance in both path tracking and driving stability, and has better stability of rollover under emergency.

INDEX TERMS emergency collision avoidance, rear wheel steering, rollover control, intelligent vehicle

I. INTRODUCTION

At present, obstacle avoidance or collision avoidance systems have been developed and became one of the principal priorities for most intelligent vehicle manufacturers because it is a key technology for the self-driving vehicle, however, it also faces many challenges. The intelligent vehicle is a complex multi-input/output system due to the fusion of multi-sensors information with parameter uncertainties and the coupled phenomena of longitudinal and lateral dynamics, which evidently are the combination of cornering and braking maneuvers [1]. The advanced driving assistant systems (ADAS) such as adaptive cruise control (ACC), forward collision warning (FCW), and active emergency brake (AEB), can enhance driving safety [2]. However, vehicle rollover happens frequently and particularly prominent in highway vehicle during emergency collision avoidance (ECA), which has raised much concern for the increasing fatal rollover accidents. And the increased popularity of the high center of gravity (CG) vehicles such as sport utility vehicle (SUV) are subjected to more fatal accidents because of their intrinsic dynamics [3]. The main cause of the vehicle rollover is due to the vehicle manoeuvring at limit handling conditions [4]. The National Highway Traffic Safety Administration (NHTSA) estimates that about 88% collisions in the United States are caused by driver factor. Moreover, the expected path of the intelligent vehicle to achieve better rollover stability is often ignored, which may lead to the deviation of the planed path under emergency. Thus, for intelligent vehicles, designing of an effective obstacle avoidance control model suitable for highway under emergency is a key issue.

Vehicle driving safety is mainly dependent on electronic stability control (ESC), which has been widely applied to passenger cars [5-7]. For SUV vehicle with high CG, rollovers maybe still occur easily even with ESC [8]. Thus, many approaches have been adopted to prevent rollovers, such as active steering [9-10], active suspension or semi-

active suspension [11-12], active differential braking [8,13], and active stabilizer mechanism [14]. The active stabilizer mechanism and active suspension are two direct ways for the restraining of vehicle roll motion. Highway emergency obstacle avoidance mainly adopts emergency steering to avoid obstacles, and it is easy to generate large lateral acceleration and cause rollover [15]. Facts proved that it is effective to prevent rollover indirectly by decreasing the lateral acceleration of a vehicle. Braking the target wheels or utilizing active steering are possible ways to reduce the lateral acceleration when the vehicle is in danger of rollover. Due to the cost of the active suspension and its limited effectiveness for rollover prevention, braking target wheels or active steering is preferable [13].

For path planning methods at ECA, parametric curve is a typical method. It mainly uses B spline curves, polynomial functions, etc. Galvani et al. [16] designed a trajectory of vehicle based on optimal control, which considered the factors of time and lateral acceleration. Daniel et al. [17] proposed a path planning method based on B spline curves, which considered the kinematic and dynamic constraints of vehicle and geometric constraints of road. To achieve an effectiveness path tracking control strategy at ECA, many scholars have proposed various control methods [18–20]. The PID method was used in [18] to construct a lateral feedback controller and to achieve lateral motion control. Shim et al. [19] presented a motion control system, which tracks the determined evasive path based on MPC method. Llorca et al. [20] provided an ECA system using fuzzy controller to imitate the driver's behave. Wang et al. [21] proposed an integrated active steering and active braking controller based on model predictive control (MPC) and sliding mode control (SMC). The integrated controller can ensure the vehicle tracking the expected path and achieving rollover prevention. However, real-time highway path tracking remains many challenges on the complex road with dynamic obstacles. If the obstacle is ahead of the vehicle directly, the vehicle control system must decide immediately to how to avoid it, and an emergency steering is mainly adopted.

Multi-sensor information fusion technique has been applied in many fields, which can integrate a large amount of data and knowledge and the data may be independent or redundant, and can be obtained by different sensors at the same time or at different times [22]. To improve the efficiency and safety in highway ECA of vehicle, an active safety collaborative control system integrated with ACC, rear steering control (RSC), and rollover braking control (RBC) is developed. Active rear wheel steering based on lateral acceleration feedback and active braking control strategies based on fuzzy PID are added into the control model to enhance driving stability.

An SUV vehicle is selected as the control subject for study. The remainder of this paper is organized as follows. In Section 2, the vehicle dynamic models and the driver are established. The proposed active obstacle avoidance system with active rear wheel steering is established in Section 3. The proposed active obstacle avoidance system with active rollover braking control under emergency is demonstrated by the combined simulation based on CarSim and Simulink software in Section 4. Section 5 presents the conclusions of the work.

II. DRIVER-VEHICLE SYSTEM MODELING

It is necessary to establish the driver-vehicle system dynamic model before researching the active obstacle avoidance controller for intelligent vehicles. The system models mainly include the driver model and vehicle model.

A. DRIVER SYSTEM MODEL

A three-point preview driver model [23] is established as shown in Figure 1.

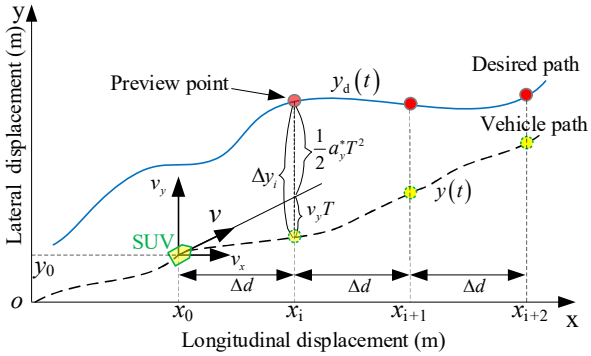

Figure 1. Steering control by preview-follower theory.

In the three-point preview driver model, The driver scans through the desired path within a finite distance Δd. The real position of the SUV vehicle respect to the global coordinates **x, y** is derived as

$$\begin{cases} y = y_0 + v\int_0^t \cos(\beta+\varphi)\mathrm{d}t \\ x = x_0 + v\int_0^t \sin(\beta+\varphi)\mathrm{d}t \end{cases}, \tag{1}$$

where, $\varphi = \varphi_0 + \int_0^t \gamma \mathrm{d}t$, x_0, y_0, and φ_0 are the vehicle positions when t=0, and v, γ, β are the vehicle speed, yaw rate, slip angle respectively.

The lateral position error in the coordinate system between the vehicle path and the desired path in the ith preview point can be written as

$$\Delta y_i = y_{\mathrm{di}}(t+T) - y_i(t), \tag{2}$$

where $y_{\mathrm{di}}(t)$ is the desired lateral displacement in the ith preview point, $y_i(t)$ is the actual lateral displacement, T is the preview time and $T = \Delta d / v_x$, v_x is the vehicle longitudinal speed.

It is assumed that the Δy_i can eliminate after T , and the following relations can be obtained:

$$y_{\mathrm{d}}(t) = y(t+T) + \Delta y_i^* , \tag{3}$$

The ideal lateral displacement error Δy_i^* can be rewritten as

$$\Delta y_i^* = y(t+T) - y_{\mathrm{d}}(t) = \dot{y}(t)T + \frac{1}{2}a_y^* T^2 , \tag{4}$$

then

$$a_y^* = \frac{2}{T^2}\left(y(t+T) - y(t) - \dot{y}(t)T\right), \tag{5}$$

where a_y^* is the ideal lateral acceleration.

To obtain a_y^*, the ideal steering angle δ^* should be input as:

$$\delta^* = \frac{a_y^*}{G_{ay}}, \tag{6}$$

where G_{ay} is steady state gain of vehicle lateral acceleration for vehicle steering wheel angle.

According to two degree-of-freedom (DOF) vehicle dynamics model, as shown in Figure 2.

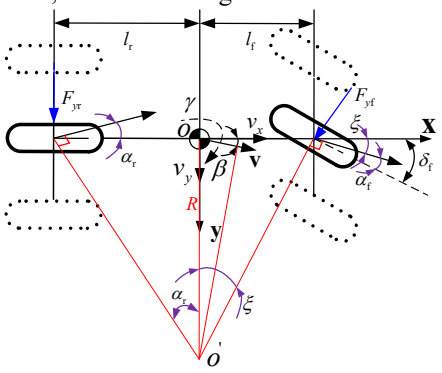

Figure 2. Two DOF vehicle dynamics model.

The dynamic equations of the vehicle lateral and yaw motion can be described, respectively, as

$$ma_y = F_{yf}\cos\delta_f + F_{yr}, \tag{7}$$

$$I_z\dot{\gamma} = l_f F_{yf}\cos\delta_f - l_r F_{yr}, \tag{8}$$

$$\xi \approx \tan\xi = \frac{v_y + l_f\gamma}{v_x}, \tag{9}$$

where $a_y = \dot{v}_y + v_x\gamma$, m is the vehicle mass, v_y is the vehicle lateral velocity, I_z is the yaw moment of inertia; F_{yf}, F_{yr} is the lateral force by the front and rear tire, l_f and l_r are the distance from CG to front and rear axle, respectively. The slip angle by the front and rear tire can be written as

$$\alpha_f = \delta_f - \xi = \delta_f - \frac{v_y + l_f\gamma}{v_x}, \tag{10}$$

$$\alpha_r = \frac{-v_y + l_r\gamma}{v_x}, \tag{11}$$

where δ_f is the front wheel steering angle.

To facilitate the design of driver model, the linear tire model is established as

$$F_{yf} = k_f\alpha_f, \tag{12}$$

$$F_{yr} = k_r\alpha_r, \tag{13}$$

where k_f and k_r are the cornering stiffness by the front and rear tires. Hence, the following equation can be got as

$$\begin{cases} m\left(\dot{v}_y + v_x\gamma\right) = k_f\delta_f - \left(k_f + k_r\right)\dfrac{v_y}{v_x} - \left(l_f k_f - l_r k_r\right)\dfrac{\gamma}{v_x} \\ I_z\dot{\gamma} = l_f k_f\delta - \left(l_f k_f - l_r k_r\right)\dfrac{v_y}{v_x} - \left(l_f^2 k_f + l_r^2 k_r\right)\dfrac{\gamma}{v_x} \end{cases}. \tag{14}$$

When vehicle driving at steady state steering, $\dot{\gamma}$ =0, $\dot{v}_y$ =0, eliminate v_y, hence, the steady state gain of yaw rate response and front steer input is realized as follow:

$$\gamma = \frac{v_x}{l\left(1 + Kv_x^2\right)}\delta_f, \tag{15}$$

where $K = \dfrac{m\left(l_r k_r - l_f k_f\right)}{l^2 k_f k_r}$, K is the understeer gradient and $K\in$[0.002,0.004] s^2/m^2.

For realistic values of the vehicle lateral velocity v_y in absolute value are much smaller than the longitudinal velocity v_x. This means the total velocity $\mathbf{v}=\sqrt{v_x^2 + v_y^2}$ of the CG can be approximated by v_x. Since v = $R\gamma$, it also can be got the relationship of yaw rate response and lateral acceleration as follow:

$$a_y = \gamma^2 R = \left(\frac{v_x}{R}\right)^2 R = \gamma\left(\frac{v_x}{R}\right)R = \gamma v_x, \tag{16}$$

where R is the turning radius.

Then, the desired lateral acceleration can be defined as

$$a_y^* = \frac{v_x^2}{l\left(1 + Kv_x^2\right)}\delta_f^*. \tag{17}$$

Substitute Eq. (17) into Eq. (6), the following steady state gain is obtained:

$$G_{ay} = \frac{v_x^2}{lI\left(1 + Kv_x^2\right)}, \tag{18}$$

where I is steering gear ratio, $I=\delta/\delta_f$.

B. CARSIM SUV VEHICLE MODEL AND SIMULATION

The standard vehicle simulation software of Carsim is used to validate the effectiveness of the proposed control strategy. The driver model or the obstacle avoidance controller can be designed in Matlab and it's easy to realize CarSim-Simulink co-simulation tests through the vehiclesim browser interface. Figure 3 shows the SUV simulated in CarSim and the important parameters of the Carsim vehicle model are shown in Table 1.

Figure 3. CarSim vehicle model.

TABLE 1. IMPOTENT PARAMETERS FOR SUV.

Parameters	Value
Front, rear unsprung mass m_{uf}, m_{ur}	125, 125 kg
Sprung mass, total mass m_s, m	2000, 2500 kg
Height of CG from ground h	0.781 m
Height of CG from roll center h_s	0.381m
Distance from CG to front, rear axle l_f, l_r	1.3, 1.5 m
Wheel track width t_w	1.725 m
Wheel rolling radius r_w	0.400 m
Acceleration due to gravity g	9.81m/s^2
Yaw moment of inertia about yaw axis I_z	3524.9 kg · m^2
Roll moment of inertia about roll axis I_x	846.6 kg · m^2
Wheel moment of inertia J_w	2 kg · m^2

A 265/70R17 radial pneumatic tire (300 kPa) is selected as the sample of tire mechanical properties. The cornering conditions of the tire model are illustrated in Figure 4.

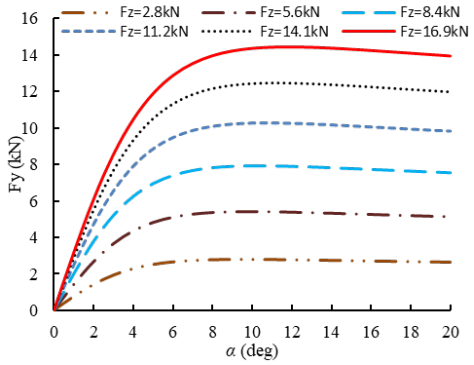

Figure 4. Lateral tire force at different slip angles and different vertical tire forces.

However, the driver steering control system has to be designed considering the tire characteristics of cornering stiffness, which are determined by Eq.(12) and Eq.(13). For the design of the steering control model, the front and rear axle cornering stiffness k_f, k_r are set 114650 N/rad, 103184 N/rad, respectively.

The preview time T influenced tracking performance and stability a lot. In a normal ECA system, multiple objectives with respect to tracking capability and driving stability should be ensured. When steering control model with a long preview time, the vehicle's state response is more stable obviously, but a worse performance in path tracking. On the contrary, when the control model with a smaller preview time, path tracking performance is best but the vehicle is easy to become unstable [24]. In this causes, define a safety coefficient of preview range ψ_s, $\psi_s = \Delta d/\Delta d_{safe}$, Different driving styles have different preview distances. Three levels of low, moderate and high are used to analyze the influence of preview distances on vehicle tracking performance and stability. The responses of the yaw rate and the roll angle have been used as the index of driving stability evaluation. To reflect preview range of different people, set $\psi_s = \{0.5,1,1.5\}$ and Δd_{safe}=30 m. A block diagram of the architecture for driver vehicle model based on lateral acceleration feedback is shown in Figure 5.

For path planning methods, parametric curve is a typical method. This work mainly focuses on the path tracking control strategies and the path planning algorithms are no longer given here, which can be referred to Wang et al. [21]. The path tracking, steering angle, and stability evaluation index at different preview ranges are shown in Figure 6.

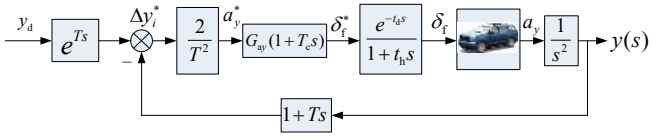

Figure 5. Architecture of the driver vehicle model.

It is clear from Figure 6 that as the vehicle steering control model using a high coefficient of preview range, the vehicle steering output is obviously smoother and more stable, but the path tracking performance becomes worse, which means that the relative lateral displacement error is increased. When ψ_s =0.5, path tracking error is best, but the steering output lost grip and vehicle becomes unstable. So, the coefficient of preview range is set at a moderate level in this article.

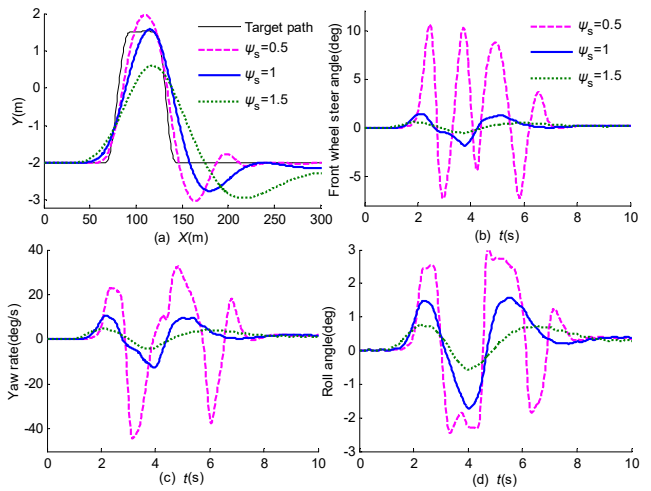

Figure 6. Path tracking and handing properties comparisons at different preview range: (a) Path tracking comparison; (b) Steering angle comparison; (c) Yaw rate comparison; (d) Roll angle comparison.

III. THE DESIGN OF PROPOSED CONTROL STRATEGY

The proposed active obstacle avoidance system with active rear wheel steering, can not only accomplish multi-objective adaptive cruise control considering tracking capability, but also improved driving stability under collision avoidance. Its hierarchical control architecture is illustrated in Figure 7. It is assumed that the measurement accuracy of the sensors can meet the requirements.

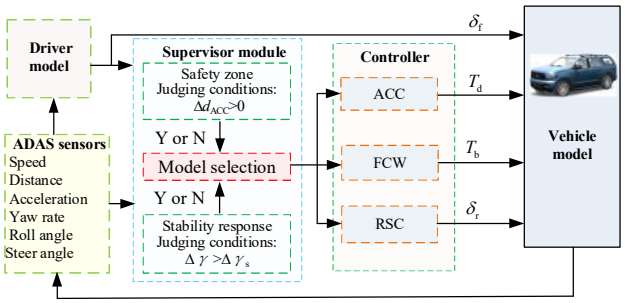

Figure 7. Structure of the active obstacle avoidance system.

A. ADAS SENSORS MODEL FOR ACC AND FCW

The adaptive cruise control (ACC) system is introduced in this part, which not only addresses the issues of tracking capability, fuel economy during car-following process but also ensures effective collision avoidance and the lateral stability of the following vehicle [25]. The moving obstacles can be programmed to imitate traffic vehicles in advanced driver assistance systems (ADAS) involving automated controls in response to detected interactions with other vehicles.

For the ACC controller, speed control is one of the key issues for the autonomous driving study. Research in vehicle speed following problems mainly focus on throttle control and brake control. The control goals of the vehicle's throttle and brake are to manage the vehicle speed with the target speed and space. The speed control algorithm is established based on a uniform accelerator for the roads it travels on. The expected safety velocity v_{xd} can be obtained by intelligent network connection technology at any road position. In the process of longitudinal speed following control, it is assumed that the vehicle can reach the desired speed after T by an ideal longitudinal acceleration a_x*, then

$$a_x^* = \left(v_{xd} - v_x\right)/T\,, \tag{19}$$

To achieve the ideal longitudinal acceleration a_x^*, a conventional PID controller is adopted by regulating the throttle and brake. The design uniform accelerator of the speed controller is as follows:

$$T_d^* = \left(K_p + K_d s + \frac{K_i}{s}\right)\left(a_x^* - a_x\right), \tag{20}$$

where T_d^* is the required torque from throttle and brake actuators.

The main coupling effect of speed control and steering control comes from the influence of the speed on the lateral dynamic characteristics, that is, the gain of lateral acceleration for steering wheel angle is the function of the speed. Therefore, the decoupling of the vehicle speed control and steering control can be realized by continuously updating the gain G_{ay} according to the change of vehicle speed. Define a nonlinear model as

$$G_{ay} = f\left(v_x\right), \tag{21}$$

where f is the function of the speed. We assume the driver behaves in an optimal fashion, in other words, the coefficient of preview range is set at a moderate level.

Two indexes consisting of the distance error Δd_{ACC} and the velocity error Δv_{ACC} between the preceding vehicle and the following vehicle to indicate the tracking capability of vehicle-following are calculated as followings:

$$\Delta v_{ACC} = v_p - v_x\,, \tag{22}$$

$$\Delta d_{ACC} = d_s - d_x\,, \tag{23}$$

where d_s is the desired distance, v_p is the longitudinal speed of the preceding vehicle.

According to the related standards which are published by National Highway Traffic Safety Administration (NHTSA), the European Union (EU) and the International Organization for Standardization (ISO), the safe collision time is a constant value of 2.4 s, and there is no weighting factor based on different drivers. However, different driving styles have different forward anti-collision risk coefficient ζ_s. Define a safe collision time

$$T_{SC} = \zeta_s \frac{\Delta d_s}{\Delta v_{ACC}}\,. \tag{24}$$

According to the multiple forward collision warning (FCW) tests of different vehicle. If T_{SC}=2.4 s, v_p=35 km/h, v_x=110 km/h, ζ_s =1, then, Δd_s=2.4×(110 -35)/3.6=50 m. Three levels (Low, moderate, high) are used to analyze the influence of forward anti-collision risk coefficient on vehicle tracking performance and stability. To reflect the risk coefficient of different people, set ζ_s = {0.8,1,1.2}. The moderate level is 50 m, which means the distance range for the FCW sensor is 50 m. But, of course, the range of the sensors can be adjusted so that they can be used in a real vehicle. A block diagram of the architecture for the ACC+FCW model based on longitudinal acceleration feedback is shown in Figure 8. The forward anti-collision risk distance, path tracking, and stability evaluation index at different anti-collision risk coefficients are shown in Figure 9.

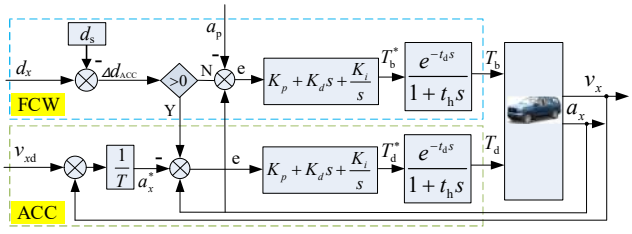

Figure 8. A block diagram of the architecture for ACC+FCW model.

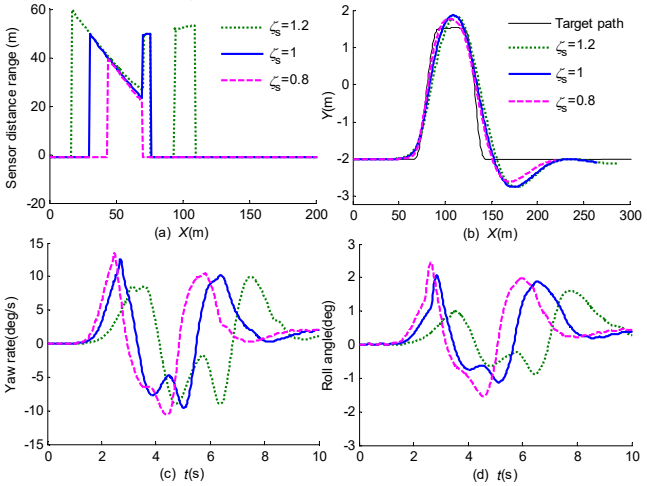

Figure 9. Path tracking and stability evaluation index at different anti-collision risk coefficient: (a) Forward anti-collision risk comparison; (b) Path tracking comparison; (c) Yaw rate comparison; (d) Roll angle comparison.

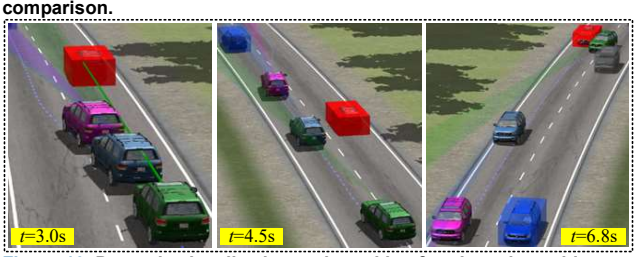

Figure 10. Dynamic visualization path tracking for obstacle avoidance.

This article has been accepted for publication in a future issue of this journal, but has not been fully edited. Content may change prior to final publication. Citation information: DOI 10.1109/ACCESS.2020.3029042, IEEE Access

It is clear from Figures 9 and 10 that as the ACC+FCW control model using a high coefficient of sensors range, the vehicle response of yaw rate and roll angle are obviously more stable, but the path tracking efficiency becomes worse, which means that the fuel economy is increased. When ζ_s =0.8, path tracking efficiency is best, but the driving stability becomes worse. So, the coefficient of sensors range is set at a moderate level in this article. The longitudinal speed of following vehicle at different anti-collision risk coefficient is presented in Figure 11, and the corresponding brake moment of four wheels controlled by ACC+FCW is shown in Figure 12.

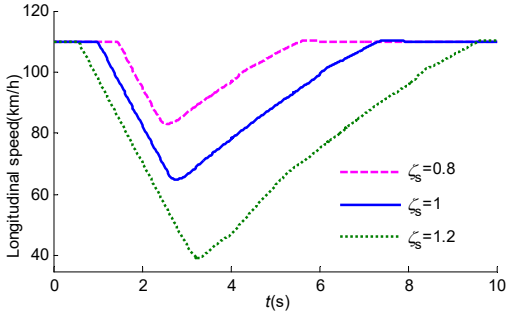

Figure 11. Vehicle longitudinal speed response at different ζ_s.

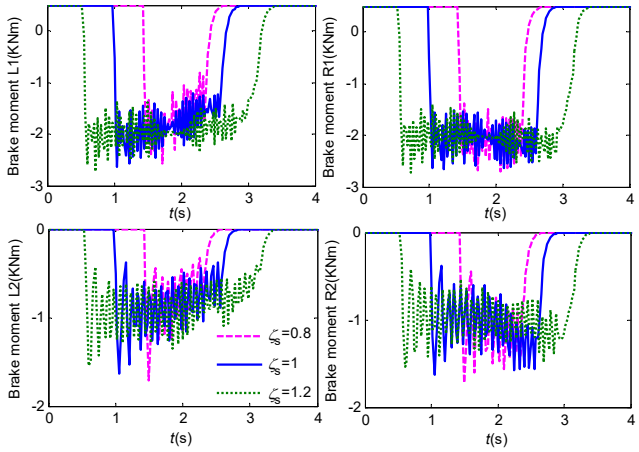

Figure 12. Brake moment of four wheels controlled by ACC+FCW at different ζ_s.

In Figure 12, it can be concluded that the ACC brake the vehicle at 0.5s and the vehicle speed is reduced to 40km/h when ζ_s =1.2, which is because the active braking signal of ACC starts to work at 60 m between vehicles. It is conservative for most aggressive drivers in practice. The proposed ACC+FCW controller can not only avoid collision effectively but also guarantee the lateral dynamics stability in ECA.

B. Rear wheel steering controller

For a front wheel steering vehicle, the rear tires could only generate a certain slip angle resulted from the yaw and sideslip motion of vehicle. However, both steering angles of the front and rear tires has more advantage on directly controlling of vehicle lateral movement. Directly rear wheel steering can help to reduce the vehicle's yaw motion and improve the driving stability. The two DOF linear vehicle model will be used to design a rear wheel steering controller (RSC), which will calculate a steering angle of the rear wheels depending on vehicle yaw rate response.

It is used quite often of two DOF linear vehicle model in studies on active steering. The slip angle by the rear tire can be written as

$$\alpha_r = \delta_r - \frac{v_y - l_r\gamma}{v_x} \quad , \tag{25}$$

where δ_r is the steering angles of the rear wheels. Eq.(14) can be combined into two coupled first order differential equations.

$$\begin{cases} m\dot{v}_y + \left(k_f + k_r\right)\dfrac{v_y}{v_x} + \left(mv_x + \dfrac{l_f k_f - l_r k_r}{v_x}\right)\gamma = k_f\delta_f + k_r\delta_r \\ I_z\dot{\gamma} + \dfrac{l_f^2 k_f + l_r^2 k_r}{v_x}\gamma + \dfrac{l_f k_f - l_r k_r}{v_x}v_y = l_f k_f\delta_f - l_r k_r\delta_r \end{cases} , \tag{26}$$

Written in state space form with state x=[v_y, γ], input u=[δ_f, δ_r], the relevant equations are given by:

$$\dot{\mathbf{x}} = \mathbf{A}\mathbf{x} + \mathbf{B}\mathbf{u} \quad , \tag{27}$$

where,

$$\mathbf{A} = \frac{-1}{v_x}\begin{bmatrix} \dfrac{k_f + k_r}{m} & \dfrac{l_f k_f - l_r k_r}{m} + v_x^2 \\ \dfrac{l_f k_f - l_r k_r}{I_z} & \dfrac{l_f^2 k_f + l_r^2 k_r}{I_z} \end{bmatrix}, \mathbf{B} = \begin{bmatrix} \dfrac{k_f}{m} & \dfrac{k_r}{m} \\ \dfrac{l_f k_f}{I_z} & -\dfrac{l_r k_r}{I_z} \end{bmatrix} .$$

The characteristic equation $det(s\mathbf{I}\text{-}\mathbf{A}) = 0$ of the state space system is given by

$$\det(s\mathbf{I} - \mathbf{A}) = \begin{vmatrix} s + \dfrac{k_f + k_r}{mv_x} & \dfrac{l_f k_f - l_r k_r}{mv_x} + v_x \\ \dfrac{l_f k_f - l_r k_r}{I_z v_x} & s + \dfrac{l_f^2 k_f + l_r^2 k_r}{I_z v_x} \end{vmatrix} = 0 , \tag{28}$$

$$\Rightarrow \begin{matrix} s^2 + \left(\dfrac{l_f^2 k_f + l_r^2 k_r}{I_z v_x} + \dfrac{k_f + k_r}{mv_x}\right)s + \dfrac{k_f + k_r}{mv_x}\cdot\dfrac{l_f^2 k_f + l_r^2 k_r}{I_z v_x} \\ -\dfrac{l_f k_f - l_r k_r}{I_z v_x}\cdot\left(\dfrac{l_f k_f - l_r k_r}{mv_x} + v_x\right) = 0 \end{matrix} , \tag{29}$$

$$\Rightarrow \begin{matrix} s^2 + \left(\dfrac{l_f^2 k_f + l_r^2 k_r}{I_z v_x} + \dfrac{k_f + k_r}{mv_x}\right)s + \\ \dfrac{l^2 k_f k_r + mv_x^2\left(l_f k_f - l_r k_r\right)}{mI_z v_x^2} = 0 \end{matrix} , \tag{30}$$

$$\Rightarrow \begin{matrix} s^2 + \left(\dfrac{l_f^2 k_f + l_r^2 k_r}{I_z v_x} + \dfrac{k_f + k_r}{mv_x}\right)s + \\ \dfrac{l^2 k_f k_r}{mI_z v_x^2}\left(1 - \dfrac{m\left(l_f k_f - l_r k_r\right)}{l^2 k_f k_r}v_x^2\right) = 0 \end{matrix} , \tag{31}$$

$$\Rightarrow s^2 + \left(\frac{l_f^2 k_f + l_r^2 k_r}{I_z v_x} + \frac{k_f + k_r}{mv_x}\right)s + \frac{l^2 k_f k_r}{mI_z v_x^2}\left(1 + Kv_x^2\right) = 0 , \tag{32}$$

where, $K=\dfrac{m\left(l_{\mathrm{r}}k_{\mathrm{r}}-l_{\mathrm{f}}k_{\mathrm{f}}\right)}{l^{2}k_{\mathrm{f}}k_{\mathrm{r}}}$. From Eq.(32), it is seen that the active four wheels steering system is unstable if $K>-1/v_x^2$, in other words, if $K<0$ and $v_x>\sqrt{-1/K}$.

In stationary situations, such as steady-state cornering, $\dot{v}_y=0$, $\dot{\gamma}=0$, eliminate v_y of Eq.(26), hence, it follows that:

$$\left[mv_x^2\left(l_{\mathrm{f}}k_{\mathrm{f}}-l_{\mathrm{r}}k_{\mathrm{r}}\right)-l^2k_{\mathrm{f}}k_{\mathrm{r}}\right]\gamma=-k_{\mathrm{f}}k_{\mathrm{r}}lv_x\left(\delta_{\mathrm{f}}-\delta_{\mathrm{r}}\right), \quad (33)$$

$$\Rightarrow\left(1+Kv_x^2\right)\gamma=\frac{v_x}{l}\left(\delta_{\mathrm{f}}-\delta_{\mathrm{r}}\right). \quad (34)$$

Likely, eliminate γ of Eq.(26), hence, it follows that

$$\left(1+Kv_x^2\right)v_y=\frac{v_x}{l}\left(l_{\mathrm{r}}-\frac{ml_{\mathrm{f}}v_x^2}{lk_{\mathrm{r}}}\right)\left(\delta_{\mathrm{f}}-\delta_{\mathrm{r}}\right)+l\left(1+Kv_x^2\right)\delta_{\mathrm{r}}, \quad (35)$$

Written in state space form as

$$\left(1+Kv_x^2\right)\begin{bmatrix}v_y\\ \gamma\end{bmatrix}=\frac{v_x}{l}\begin{bmatrix}l_{\mathrm{r}}-\dfrac{ml_{\mathrm{f}}v_x^2}{lk_{\mathrm{r}}} & l\left(1+Kv_x^2\right)\\ 1 & 0\end{bmatrix}\cdot\begin{bmatrix}\delta_{\mathrm{f}}-\delta_{\mathrm{r}}\\ \delta_{\mathrm{r}}\end{bmatrix}. \quad (36)$$

Since $v_x\approx|\mathbf{v}|=R\gamma$, and $a_y=|\mathbf{v}|^2/R\approx v_x^2/R$, Eq.(36) can be rewritten as:

$$\delta_{\mathrm{f}}-\delta_{\mathrm{r}}=\frac{\gamma l}{v_x}\left(1+Kv_x^2\right)\approx\frac{v_x}{R}\frac{l}{v_x}\left(1+Kv_x^2\right)=\frac{l}{R}\left(1+Kv_x^2\right)=\frac{l}{R}+Ka_y \quad (37)$$

It is noted that the rollover stability influenced by a_y can be improved by adjusting the steering angle of the rear wheels before reaching a critical condition.

According to Eq. (37), the active rear wheel steering system can be designed as:

$$\delta_{\mathrm{r}}=c_1\delta_{\mathrm{f}}+c_2a_y, \quad (38)$$

where, c_1=-1, c_2=K. Figure 13 shows the block diagram of the RSC.

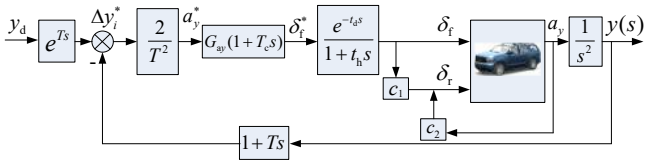

Figure 13. Block diagram of active rear wheel steering control scheme.

Driving on a busy highway, changing lanes can be very hazardous obviously. There are many blind spots, which is a problem for every driver. Ignorance the blind region while changing lane will lead to a collision with another obstacle. The steer control strategy fully addresses this situation by ensuring that the blind spots of the intelligent vehicle are clear prior to the controller attempt to change lanes. The steering angle, path tracking and stability evaluation index comparisons by rear wheel steering controller are shown in Figure 14.

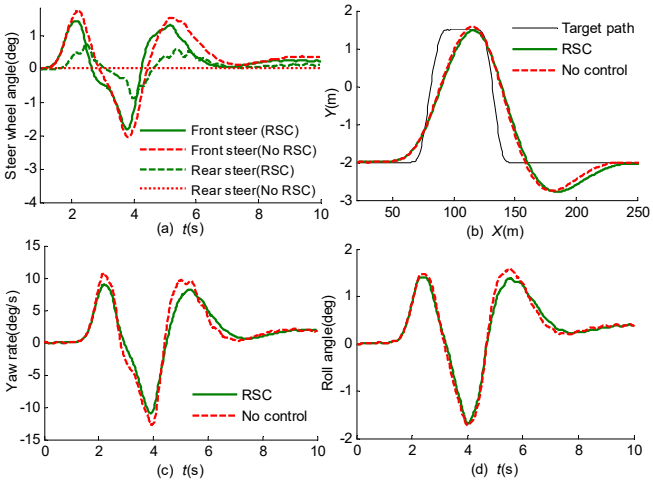

Figure 14. Path tracking and stability evaluation index by RSC: (a) Front and rear wheel steer angle comparison; (b) Path tracking comparison; (c) Yaw rate comparison; (d) Roll angle comparison.

It is clear from Figure 14 that the maximum value of yaw rate reduced -14.5 % by RSC at 3.9 s and the maximum value of roll angle reduced -14.4 % by RSC at 5.5 s. Besides, the maximum value of front steer angle reduced 21.3% by RSC at 2.1 s, however, the RSC has less influence on the path tracking performance. Which means RSC can help to reduce the vehicle's yaw and roll motion and improve the driving stability.

C. Active obstacle avoidance control strategy

To make the vehicle motion control strategy suitable for high speed path tracking with obstacle avoidance, priority will be given to the FCW controller and braking control strategy will be used even though the vehicle speed is lower than the expected speed when the Δd_x is less than the safety range of Δd_s. The rear wheel steering control and speed control are integrated into a motion control model for obstacle avoidance. The "high speed" means vehicle actual speed over 60km/h and "expected speed" means vehicle safety or allowed driving speed in this article.

The model selection methods of the control mode developed in the supervisor are as follows: According to the driver's input and vehicle status signal, the actual distance of preceding vehicle d_x and following vehicle and the actual yaw rate γ are obtained. Then, they are compared with the ideal distance d_s and the ideal yaw rate γ_s. When d_x is more than d_s ($\Delta d_{ACC}>0$), it is considered that the vehicle is in a longitudinal safe area and the speed does not need to be reduced additionally. In this case, the ACC controller is turned on only. Otherwise, the FCW controller based on active braking is turned on. When the difference between the actual yaw rate and the ideal yaw rate is less than $\Delta\gamma_s$, it is considered that the vehicle can track the expected trajectory, and the active steering controller based on rear wheel steering is closed. On the contrary, the RSC controller is turned on. Table 2 shows the switching strategy of the control mode in the supervisory decision control.

TABLE 2. SWITCHING STRATEGY OF THE CONTROL MODE IN THE SUPERVISORY DECISION CONTROL.

Control model	Selection conditions	ACC	FCW	RSC
1	$(\Delta d_{ACC}>0)$ and $(\Delta y<\Delta y_s)$	Open	Close	Close
2	$(\Delta d_{ACC}<0)$ and $(\Delta y<\Delta y_s)$	Close	Open	Close
3	$(\Delta d_{ACC}<0)$ and $(\Delta y>\Delta y_s)$	Close	Open	Open
4	$(\Delta d_{ACC}>0)$ and $(\Delta y>\Delta y_s)$	Open	Close	Open

ACC: adaptive cruise control; FCW: forward collision warning; RSC: rear steering control.

Finally, the block diagram of the proposed active obstacle avoidance system with active rear wheel steering is established in Figure 15. Firstly, both vehicles with or without ADAS control can achieve collision avoidance, which is concluded in Figure 16. The proposed FCW+ACC+RSC achieve collision avoidance at 7.5 s and the vehicle without ADAS control achieve collision avoidance at 5.1 s, which is because the vehicle with ADAS control is in full braking when the longitudinal distance of the driving vehicle and preceding vehicle is less than the desired distance. The path tracking performance and stability evaluation index comparisons by the different controller are shown in Figures 17 and 18.

It is clear from Figure 18 that the maximum value of yaw rate reduced 35% by FCW+ACC+RSC at 120 m and the maximum value of roll angle reduced 36% compared with no controlled vehicle, and the controller has a positive influence on the path tracking performance. Which means the proposed active obstacle avoidance control strategy can not only avoid collision effectively but also improve the driving stability dramatically.

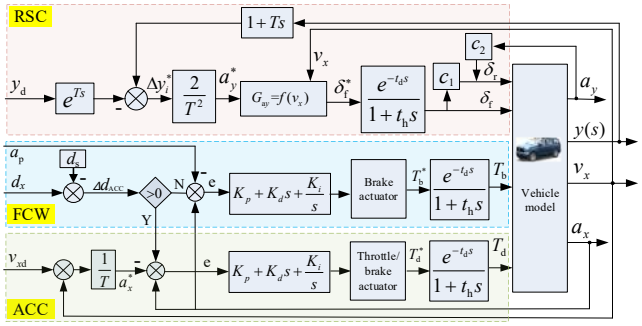

Figure 15. General control block diagram of proposed active obstacle avoidance system.

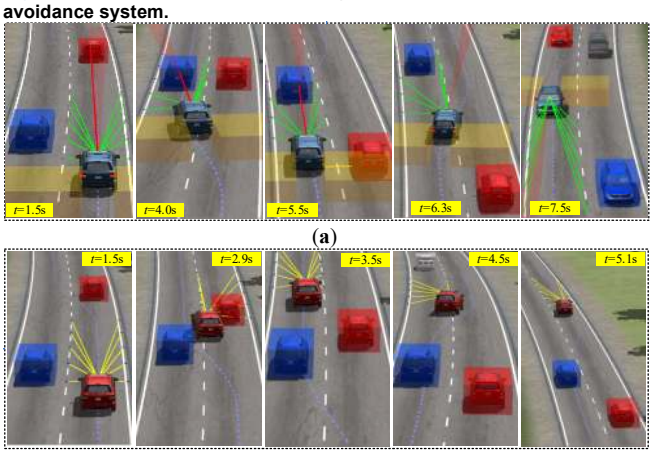

(a)

(b)

Figure 16. Dynamic visualization path tracking comparisons for active obstacle avoidance: (a) FCW+ACC+RSC; (b) No control.

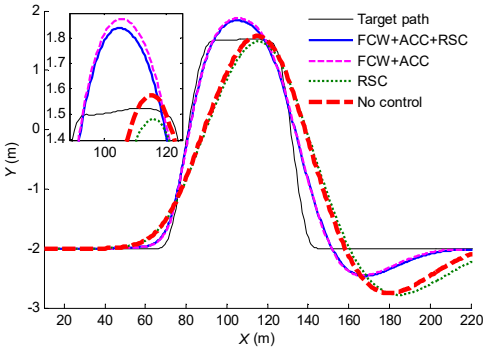

Figure 17. Vehicle path tracking performance comparisons for obstacle avoidance.

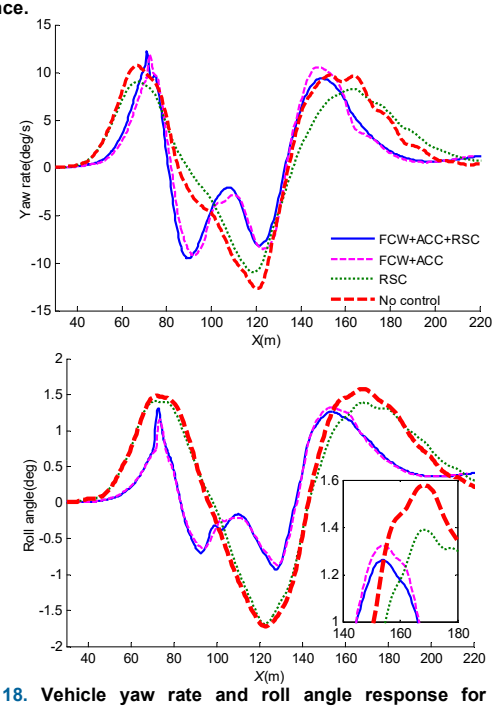

Figure 18. Vehicle yaw rate and roll angle response for obstacle avoidance.

IV. ACTIVE OBSTACLE AVOIDANCE SYSTEM WITH ROLLOVER CONTROL

For SUV vehicle with high CG, rollovers maybe still occur easily even with FCW+ACC+RSC system. The proposed active obstacle avoidance system with rollover braking control (RBC), can not only accomplish tracking capability but also avoid the rollover accident effectively under emergency collision avoidance. Its hierarchical control architecture is illustrated in Figure 19.

A. Rollover prediction index

For rollover prediction, load transfer ratio (LTR) is a commonly used rollover index, as follows

$$LTR = \frac{F_{zr} - F_{zl}}{F_{zr} + F_{zl}}, \tag{39}$$

where, F_{zl}, F_{zr} are left, right wheel vertical loads. By analyzing the roll stability mechanism of the vehicle, the LTR can be rewritten as:

$$LTR=\frac{2h}{t_w}\left[\frac{a_y}{g}+\sin\phi\right]. \quad (40)$$

A new rollover prediction index of PLTR is defined as

$$PLTR_{t_0}(\Delta t)=LTR(t_0)+\dot{LTR}(t_0)\cdot\Delta t\,, \quad (41)$$

where t_0 is the time at the moment, Δt is the roll preview time. Substitute Eq. (40) into Eq. (41), the following equation is obtained:

$$PLTR_{t_0}(\Delta t)=LTR(t_0)+\frac{2h}{t_w}\cdot\frac{d}{dt}\left[\frac{a_y}{g}+\sin\phi\right]\cdot\Delta t\,. \quad (42)$$

It assumes that $\sin\phi\approx\phi$, Eq. (42) can be simplified as:

$$PLTR_{t_0}(\Delta t)=\frac{2h}{t_w}\left[\frac{a_y}{g}+\phi\right]+\frac{2h}{t_w\cdot g}\left[\dot{a}_y+g\cdot\dot{\phi}\right]\cdot\Delta t\,. \quad (43)$$

By 2-DOF model, the lateral acceleration can be further estimated as follows,

$$ma_y=k_f\delta_f+k_r\delta_r-\left(k_f+k_r\right)\frac{v_y}{v_x}-\frac{l_fk_f-l_rk_r}{v_x}\gamma\,, \quad (44)$$

from Eq. (44), it follows,

$$ma_y=-C_0\beta-C_1\frac{\gamma}{v_x}+k_f\delta_f+k_r\delta_r\,, \quad (45)$$

where $\beta=\frac{v_y}{v_x}$, $C_0=k_f+k_r$, $C_1=l_fk_f-l_rk_r$.

The derivative of Eq. (45) can be written as

$$m\dot{a}_y=-C_0\dot{\beta}-C_1\frac{\dot{\gamma}}{v_x}+k_f\dot{\delta}_f+k_r\dot{\delta}_r\,, \quad (46)$$

where $\dot{\beta}=\frac{\dot{v}_y}{v_x}=\frac{a_y-\gamma v_x}{v_x}$.

Then, the lateral acceleration derivative in the second term can be further rewritten as

$$\dot{a}_y=\frac{-C_0\left(a_y-\gamma v_x\right)-C_1\dot{\gamma}}{m\cdot v_x}+\frac{k_f\dot{\delta}_f+k_r\dot{\delta}_r}{m}\,, \quad (47)$$

Hence, $\dot{a}_y$ can be replaced by Eq. (47) and substituting it into Eq. (43), finally, the final form of the improved PLTR is shown as follows:

$$PLTR'_{t_0}=\frac{2h}{t_w}\left[\frac{a_y}{g}+\phi\right]+\frac{2h}{t_wg}\left[\frac{-C_0\left(a_y-\gamma v_x\right)-C_1\dot{\gamma}}{m\cdot v_x}+\frac{k_f\dot{\delta}_f+k_r\dot{\delta}_r}{m}+g\dot{\phi}\right]\cdot\Delta t \quad (48)$$

B. Rollover braking control strategy

If the steering wheel angle is too large or the speed is too high, the vehicle may rollover in obstacle avoidance under emergency. Using the PID control strategy, the active braking model is established based on rollover prediction. To achieve the ideal braking torque when the PLTR exceeds the safety threshold, a fuzzy controller is adopted to self-adjust different driving conditions on the foundation of a traditional PID controller. Here, an interval changing of PID parameters ($\triangle K_p$, $\triangle K_d$, $\triangle K_i$) is calculated with fuzzy logic. The braking torque of the rollover controller is:

$$T_b^*=\left(K_p+\Delta K_p\right)e_r+\left(K_i+\Delta K_i\right)\int_0^t e_r dt+\left(K_d+\Delta K_d\right)\frac{de_r}{dt}\,, \quad (49)$$

where, $e_r=PLTR-PLTR_s$.

Figure 19 shows the block diagram of the RBC scheme.

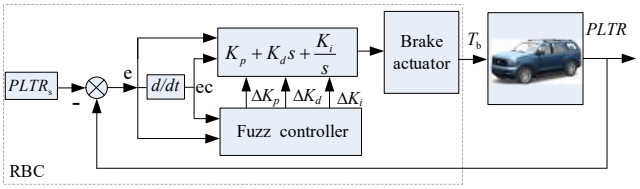

Figure 19. Block diagram of Fuzzy-PID rollover control.

For the design of fuzzy control, five conditions are considered for fuzzification whose linguistic variables are set as PM (very high), PS (high), ZO (normal), NS (low), NM (very low). Gaussian membership function is used for each variable, and the fuzzy logic controller has two inputs of e and ec. The membership functions are presented in Figure 20.

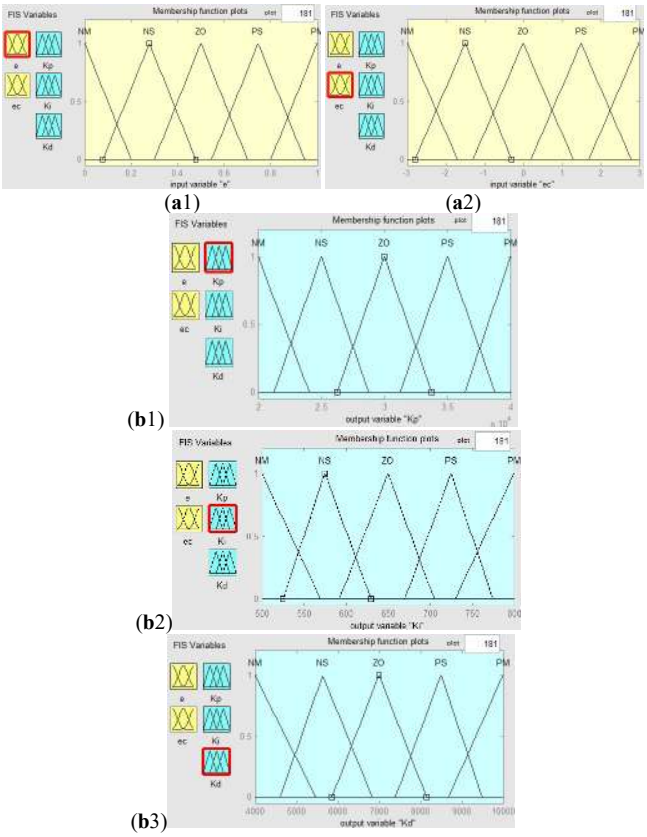

Figure 20. Membership functions for rollover control in fuzzy controller: (a1) Input variable e; (a2) Input variable ec; (b1) Output variable ΔK_p; (b2) Output variable ΔK_i; (b3) Output variable ΔK_d.

Second, the fuzzy rules base describes the relationships between status variables and control parameters. The fuzzy control rules are given in Table 3. Third, an inference method of Mamdani and a centroid defuzzification method are used for the design of fuzzy controller.

This article has been accepted for publication in a future issue of this journal, but has not been fully edited. Content may change prior to final publication. Citation information: DOI 10.1109/ACCESS.2020.3029042, IEEE Access

Table 3. Fuzzy rules of $\triangle K_P$, $\triangle K_I$, $\triangle K_D$.

(**a**). $\triangle K_P$		ec				
		NM	NS	ZO	PS	PM
e	NM	PM	PM	PS	PS	ZO
	NS	PM	PM	PS	ZO	NS
	ZO	PM	PS	ZO	NS	NM
	PS	PS	ZO	NS	NS	NM
	PM	ZO	NS	NM	NM	NM
(**b**). $\triangle K_I$		ec				
		NM	NS	ZO	PS	PM
e	NM	NM	NM	NS	NS	ZO
	NS	NM	NS	NS	ZO	PS
	ZO	NM	NS	ZO	PS	PS
	PS	NS	ZO	PS	PS	PM
	PM	ZO	PS	PS	PM	PM
(**c**). $\triangle K_d$		ec				
		NM	NS	ZO	PS	PM
e	NM	PM	PM	PS	PS	ZO
	NS	PM	PM	PS	ZO	NS
	ZO	PM	PS	ZO	NS	NM
	PS	PS	ZO	NS	NS	NM
	PM	ZO	NS	NM	NM	NM

In order to verify the effectiveness of the PLTR by Eq. (48), the different initial speed during the same "Sine" input maneuver is conducted. The conditions of PLTR transient response at different initial speed are shown in Figure 21.

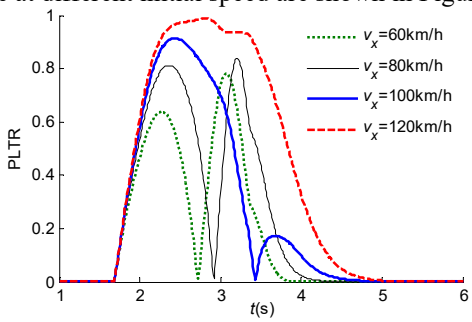

Figure 21. PLTR comparisons at different initial speed.

It can be seen from the figure, with the increase of vehicle speed, the rollover risk has also increased. Specifically, when the vehicle speed is larger than 100 km/h during the same steering input, lift-off occurs at t = 2.45 s, and the rollover index PLTR can well estimate up to that point.

Severe braking of the vehicle under emergency will also cause the wheels to lock, and resulting in loss of control. To prevent the wheels from locking, the integrated obstacle avoidance control algorithm also combines anti-lock brake control (ABS). Since the ABS modeling is not the key content in this paper, the details are no longer given here, which can be referred to Li et al [13].

To verify the effectiveness of the proposed fuzzy PID rollover control strategy for obstacle avoidance under emergency, it assumed that the FCW+ACC+RSC is out of work. The initial vehicle speed v_x is 110 km/h. The obstacle avoidance distance is 40 m and the value of lane width is 3.85 m. Another controller compared with fuzzy PID is called traditional PID. The dynamic visualization path and speed tracking for obstacle avoidance under emergency is shown in Figure 22, and the threshold value of the rollover evaluation index $PLTR_s$ is 0.7. The braking torques, path tracking, and stability evaluation index comparisons by fuzzy PID and traditional PID rollover braking controllers are shown in Figure 23.It can be found in Figure 23 that the peak values of the yaw rate and roll angle are cut down by the rollover control model compared with no control model because of the additional braking control algorithm by the measurement of rollover prediction. Whereas, the path tracking error for obstacle avoidance is also improved by rollover braking control strategy. The results in Fig. 23(d) show that the peak values of vehicle roll angle by fuzzy PID rollover control, by PID rollover control only, no rollover control are about -3.25 deg, -2.91 deg, and -2.80 deg respectively, which means the rollover stability of vehicle is significantly enhanced under emergency avoidance. It can be found in Figure 23(a) that the rollover fuzzy PID controller generates a maximum braking torque of 1200 N·m to reduce the vehicle speed actively and to prevent the occurrence of rollover. The results can prove that the proposed rollover control model has good accuracy in high speed path tracking and has better stability of rollover under emergency.

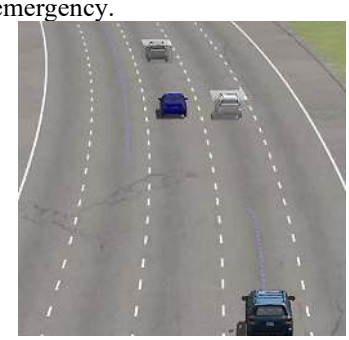

Figure 22. Dynamic visualization path and speed tracking for obstacle avoidance under emergency.

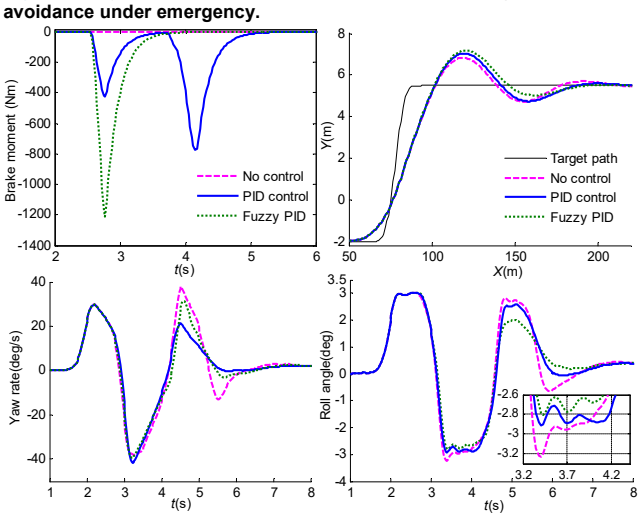

Figure 23. Path tracking and stability evaluation index by different rollover braking controllers: (a) Active braking torque comparison; (b) Path tracking comparison; (c) Yaw rate comparison; (d) Roll angle comparison.

C. Active obstacle avoidance system with RBC

The block diagram of the proposed active obstacle avoidance system with RBC is established in Figure 24. To verify the effectiveness of the proposed active obstacle

avoidance system (FCW+ACC+RSC+RBC) for highway path tracking with obstacle avoidance under emergency, the dynamic visualization path tracking for obstacle avoidance under emergency is shown in Figure 22 and the initial vehicle speed is 110 km/h. The other compared obstacle avoidance controllers are FCW+ACC, RSC, and RBC respectively. It also assumed that the FCW+ACC is out of work in RSC or RBC of the compared controllers. The path tracking performance and driving stability evaluation index comparisons by different controllers are shown in Figures 25 and 26.

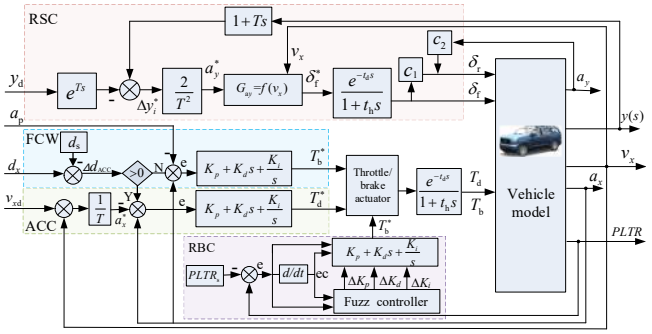

Figure 24. Block diagram of proposed active obstacle avoidance system with RBC.

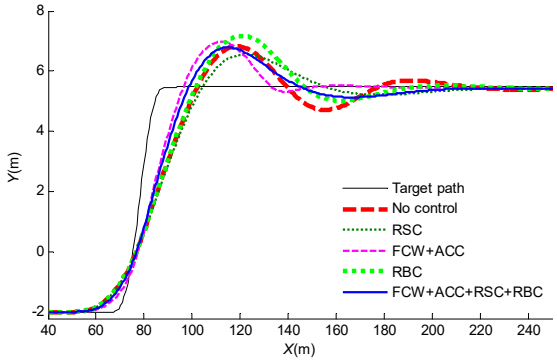

Figure 25. Vehicle path tracking performance comparisons for obstacle avoidance under emergency.

It can be found from Figure 26(b) that reduction in peak value of roll angle in case of FCW+ACC+RSC+RBC is more than 26 and 13% in case of RSC compared with no controlled vehicle, which means the proposed active safety collaborative control strategy can easier adjust the active obstacle avoidance system in rollover prediction under emergency. Figure 25 and Figure 26(a) show the path tracking and yaw rate performances of FCW+ACC+ RSC+RBC and other controllers. The maximum value of yaw rate of the no-controlled vehicle reaches -41.7 deg/s, which means that the driving vehicle tail flick accident and loses its lateral dynamics stability. However, the actual values controlled by FCW+ACC+ RSC+RBC and RSC maintain almost stable, and the maximum value of yaw rate reduced more than 50%. Whereas, the path tracking error for obstacle avoidance is also improved by the active safety collaborative control strategy. The results can prove that the proposed active obstacle avoidance controller based on active safety collaborative control has good performance in both path tracking and driving stability.

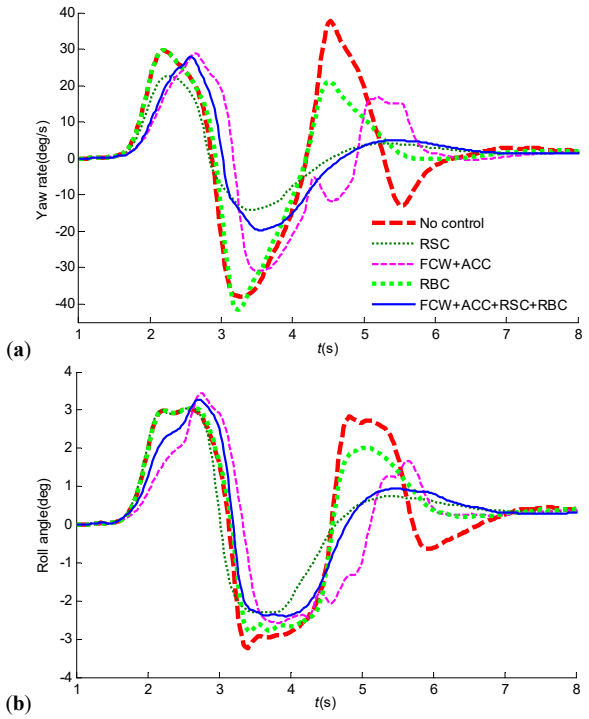

Figure 26. Vehicle state response for obstacle avoidance under emergency: (a)Yaw rate;(b) Roll angle.

From the simulation result, the controller is successfully designed and the proposed FCW+ACC+RSC +RBC shows good control ability and performance.

Experimentations will be followed in the next investigation to test and improve the control scheme further. In the first step, Hardware-in-the-Loop (HIL) in the Lab should be conducted to check and regulate the controlling laws. After that, field test will be implemented with the maneuvers in simulations to evaluate the active obstacle avoidance control system.

V. CONCLUSIONS

An obstacle avoidance control system integrated with RSC and RBC is proposed in this paper, which can not only avoid collision effectively, but also improve the driving stability dramatically. The proposed active obstacle avoidance control architecture consists of a supervisor, an upper controller, and a lower controller, and the supervisor decides which control mode to be used based on multi-sensors information of the driving vehicle. Active rear wheel steering based on lateral acceleration feedback and active braking control strategies based on fuzzy PID are added into the control model to enhance handing performance. To make the vehicle motion control model suitable for highway path tracking with obstacle avoidance under emergency, a priority was given to rollover controller even though the vehicle speed is lower than the expected speed when the PLTR exceeds the safety threshold. Finally, the Carsim-Simulink co-simulation tests validate the effectiveness of FCW+ACC+RSC+RBC. The results can be summarized as follows:

Using a high coefficient of preview range in the steering control model, the vehicle steering output is obviously

smoother and more stable, but the relative lateral displacement error increased.

Using a high coefficient of sensors range in the ACC+FCW control model, the vehicle states response of yaw rate and roll angle are obviously more stable, but the path tracking efficiency becomes worse.

RSC model and RBC model working individually has a limited impact on the improvement of the tracking performance and driving stability under emergency.

The obstacle avoidance system integrated with FCW, ACC, RSC, and RBC has good performance in both path tracking and driving stability, and especially a better stability of rollover under emergency.

REFERENCES

[1] J.H. Guo, P. Hu, and R.B. Wang, "Nonlinear coordinated steering and braking control of vision-based autonomous vehicles in emergency obstacle avoidance," *IEEE Trans Intell Transp Syst*., vol. 17, no. 11, pp. 3230-3240, 2016.

[2] L Jan, "Adaptive Cruise Control with Guaranteed Collision Avoidance," *IEEE Trans Intell Transp Syst*., vol. 20, no. 5, pp. 1897-1907, 2019.

[3] M.K. Aripin, Y.M. Sam, K.A. Danapalasingam *et al.*, "A review of active yaw control system for vehicle handling and stability enhancement," *Int J Veh Tech*., vol. 2014, pp. 1-15, 2014.

[4] M. Park, S. Lee, M. Kim, J. Lee, and K. Yi, "Integrated differential braking and electric power steering control for advanced lane-change assist systems," *Proc Inst Mech Eng Part D-J Automob Eng*., vol. 229, no. 7, pp. 924-943, 2014.

[5] X.J. Yang, Z.C. Wang, and W.L. Peng, "Coordinated control of AFS and DYC for vehicle handling and stability based on optimal guaranteed cost theory," *Vehicle Syst Dyn*., vol. 47, no. 1, pp. 57-79, 2009.

[6] J. Wu, S. Cheng, B. Liu *et al.*, "A human-machine-cooperative-driving controller based on AFS and DYC for vehicle dynamic stability," *Energies*, vol. 10, no. 11, 1737, 2017.

[7] J. Wu, X. Wang, L. Li, *et al.*, "Hierarchical control strategy with battery aging consideration for hybrid electric vehicle regenerative braking control," Energy, vol. 145, pp. 301-312, 2018.

[8] L. Li, Y.S. Lu, R.R. Wang *et al.*, "A 3-dimentional dynamics control framework of vehicle lateral stability and rollover prevention via active braking with MPC," *IEEE T Ind Electron*., vol. 64, no. 4, pp. 3389 - 3401, 2016.

[9] M. Ghazali, M. Durali, H. Salarieh, "Vehicle trajectory challenge in predictive active steering rollover prevention," *Int J Auto Tech*., vol. 18, no. 3, pp. 511-521, 2017.

[10] C.Y. Wang, W.Z. Zhao, Z.J. Xu *et al.*, "Path planning and stability control of collision avoidance system based on active front steering," *Sci China Technol Sc*., vol. 60, no. 8, pp. 1231-1243, 2017.

[11] S. Yim, Y. Park, K. Yi, "Design of active suspension and electronic stability program for rollover prevention," *Int J Auto Tech*., vol. 11, no. 2, pp.147-153, 2010.

[12] H.Q. Li, Y.Q. Zhao, F. Lin *et al.*, "Nonlinear dynamics modeling and rollover control of an off-road vehicle with mechanical elastic wheel," *J Braz Soc Mech Sci*., vol. 40, no. 2, pp. 1-17, 2018.

[13] H.Q. Li *et al.*, "Integrated yaw and rollover control based on differential braking for off-road vehicles with mechanical elastic wheel," *J Cent South Univ*., vol. 26, no. 9, pp. 2354-2367, 2019.

[14] Y. Pourasad, M. Mahmoodi-K., and M.Oveisi, "Design of an optimal active stabilizer mechanism for enhancing vehicle rolling resistance," *J Cent South Univ*., vol. 23, no. 5, pp. 1142-1151, 2016.

[15] U. Rosolia, S.D. Bruyne, and A.G. Alleyne, "Autonomous vehicle control: a nonconvex approach for obstacle avoidance," *IEEE T Contr Syst T*., vol. 25, no.2, pp. 469-484, 2017.

[16] M.Galvani, F. Biral, B.M. Nguyen *et al.*, "Four wheel optimal autonomous steering for improving safety in emergency collision avoidance manoeuvres," *Proceedings of the 13th International Workshop on Advanced Motion Control* (AMC), Yokohama, Japan, 14-16 March, pp. 362-367, 2014.

[17] J. Daniel, A. Birouche, J.P. Lauffenburger *et al.*, "Energy constrained trajectory generation for ADAS," *Proceedings of IEEE Intelligent Vehicle Symposium*. IEEE, San Diego, CA, USA, 21-24 June pp. 244-249, 2010.

[18] X.J. Zhao, and H.Y. Chen, "A study on lateral control method for the path tracking of intelligent vehicles," *Automotive Engineering*, vol. 33, no. 5, pp. 382-387, 2011.

[19] T. Shim, G. Adireddy, and H. Yuan, "Autonomous vehicle collision avoidance system using path planning and model-predictive-control-based active front steering and wheel torque control. *Proc Inst Mech Eng Part D-J Automob Eng*., vol. 226, pp. 767-778, 2012.

[20] L.D. Fernandez, V. Milanes, A.I. Parra *et al.*, "Autonomous pedestrian collision avoidance using a fuzzy steering controller," *IEEE Trans Intell Transp Syst*., vol. 12, no. 2, pp. 390-401, 2011.

[21] X. Qian, C.Y. Wang, and W.Z. Zhao, "Rollover prevention and path following control of integrated steering and braking systems," *Proc Inst Mech Eng Part D-J Automob Eng*., vol. 234, no. 6, pp. 1644-1659, 2020.

[22] X.B. Jin, S.L. Sun, H. Wei *et al.*, "Advances in multi-sensor information fusion: theory and applications," *Sensors*, vol. 18, no. 4, 1162, 2018.

[23] H.T. Ding, K.H. Guo, F. Li *et al.*, "Arbitrary path and speed following driver model based on vehicle acceleration feedback," *Chin J Mech Eng*., vol. 46, no. 10, pp. 116-120, 2010.

[24] H.Q. Li, Y.Q. Zhao, H.Y. Wang *et al.*, "Design of an improved predictive ltr for rollover warning systems," *J Braz Soc Mech Sci*., vol. 39, no.10, pp. 3779-3791, 2017.

[25] C.G. Zong, Z.J. Ji, Y. Yu *et al.*, "Research on obstacle avoidance method for mobile robot based on multisensory information fusion. *Sensors and Materials*, vol. 32, no. 4,1159, 2020.

This article has been accepted for publication in a future issue of this journal, but has not been fully edited. Content may change prior to final publication. Citation information: DOI 10.1109/ACCESS.2020.3029042, IEEE Access

Haiqing Li (M'89) received his PhD degree from Nanjing University of Aeronautics and Astronautics, China, in 2019. He is currently a lecturer in Chongqing University of Posts and Telecommunications, China. He His research interests include vehicle dynamics control and intelligent vehicle control.
E-mail: lihq@cqupt.edu.cn

Jing Li (M'96) is currently a master candidate in *Chongqing University of Posts and Telecommunications*, China. His research interest is intelligent vehicle control and mechanical signal processing.
E-mail: qindi011@163.com

Zuqiang Su. (M'87) received his PhD degree from Chongqing University, China, in 2015. He is currently an associate professor in Chongqing University of Posts and Telecommunications, China. His research interests include mechanical signal processing, machinery condition monitoring and fault diagnosis.
E-mail: suzq@cqupt.edu.cn

Xin Wang (M'89) received his PhD degree from *Xi'an Jiaotong University, China*, in 2019. He is currently a lecturer in Chongqing University of Posts and Telecommunications, China. His research interests include 3D printing and mechanical signal processing.
E-mail: wangx@cqupt.edu.cn

Jiufei Luo. (M'87) received his PhD degree from Chongqing University, China, in 2015 . He is currently an associate professor in Chongqing University of Posts and Telecommunications, China. His research interests include mechanical signal processing and intelligent vehicle control.
E-mail: luojf@cqupt.edu.cn